Sensors and Materials, Vol. 38, No. 10 (2026) 6297–6322
MYU Tokyo

S & M 4682

Transmission Loss of Mufflers with Acoustic Effects from Flow Velocity

Chang-Sheng Lin[1*] and Chin-Cheng Kang[2]

[1]Department of Mechanical Engineering, National Kaohsiung University of Science and Technology, Taiwan
[2]Outfitting Design Section, Department of Design, China Shipbuilding Corporation, Taiwan

(Received August 10, 2026; accepted October 26, 2026)

Keywords: transmission loss, quadrupole parameters, two-load method, fluid effects

To evaluate the performance of a muffler, in this study, we used the four-pole parameter theory as the measurement basis, developed a measurement configuration and solution strategy for transmission loss (TL) based on microphone-position switching, and actually applied it to the air filter assembly. To reduce the phase mismatch in the measurement process, the two-microphone transfer function method was used to correct the frequency response function to reduce the measurement error caused by the phase mismatch. In this study, LabVIEW was used to develop an algorithm for calculating TL. A relatively simple muffler was employed to measure its TL under zero-flow conditions. The analytical results were then compared with those obtained from finite element analysis to verify the effectiveness of the proposed algorithm. However, the original TL measurement did not take the fluid velocity into account and was not consistent with the actual working condition of the muffler. In this study, the TL measurement of fluid velocity was considered, and the corresponding results were compared with the measurement results without taking flow velocity into account to analyze the impact of flow velocity on TL. The experimental results obtained under both no-flow and flow conditions revealed that airflow significantly reduced the TL of the Helmholtz resonator and shifted its resonance frequency toward higher values. The single expansion chamber and the inlet extended expansion chamber increased the TL effect owing to the effect of flow rate. Only the resonant frequency of the inlet extended expansion chamber had different effects, and the TL effect at the resonant frequency decreased. The automotive muffler assembly actually tested in this study has multiple Helmholtz resonance cavities, each of which is used to deal with noise at a single frequency. The resonance behavior of the actual automotive muffler assembly differs from that of the simplified Helmholtz resonator model because of the square duct geometry, bend, and resonator configuration.

1. Introduction

Cars have become indispensable daily necessities in today's society, and the industries related to them are developing increasingly vigorously. As time goes by, the technology used in cars has become increasingly advanced, and people increasingly have higher requirements for vehicles.

*Corresponding author: e-mail: changsheng@nkust.edu.tw
https://doi.org/10.18494/SAM6575

ISSN 0914-4935 © MYU K.K.

In addition to reliability and performance, driving comfort is also one of the factors that consumers are increasingly paying attention to. The main factors that affect vehicle driving comfort are noise (N) and vibration (V), which together with harshness (H) constitute the NVH issues that the industry is concerned about. Nowadays, major domestic and foreign car manufacturers have successively invested considerable resources to address the NVH issues. If we compare the cars designed today with those built more than ten years ago, the overall comfort has been significantly improved. However, everyone's requirements for vibration and noise are very subjective. Some people may feel uncomfortable with slight vibrations of the vehicle. Therefore, in the design process, in addition to minimizing sharp and harsh noises, various car manufacturers are also gradually thinking about how to make good audio. For example, the aerodynamic noise produced by air filters and exhaust pipes may make those who hear it feel comfortable, but may also cause disgust to others. It is necessary to avoid stimulating the natural frequencies of other components and causing resonance phenomena.

The noise generated by the mufflers is mostly classified as aerodynamic noise, and the use of mufflers is one of the ways to reduce the problem of aerodynamic noise. To evaluate muffler performance, four standard indicators have been established: attenuation (ATT), insertion loss (IL), noise reduction (NR), and transmission loss (TL). Because TL will only reflect the silencing effect produced by the muffler itself, the requirements for environmental noise are smaller and more suitable for verifying the performance of the muffler. To test the noise reduction performance in a general environment, in this study, we chose TL as the test index.

The earliest application of the quadrupole parameter theory to the measurement of TL was by Munjal and Doige,[(1)] who proposed two methods for measuring the acoustic performance of pipelines, namely, the two-sound-source method and the two-load method. American Society for Testing and Materials (ASTM) uses the above-mentioned measurement method. The standard test method E1050[(2)] for acoustic materials was developed to measure the acoustic performance of pipelines. To confirm whether the TL algorithm is effective, the Helmholtz resonance chamber, the single expansion chamber, and the inlet extended expansion chamber, which are simpler than the air filter, are used as test objects. The reasons for choosing the above three mufflers are as follows. Most car mufflers have this type of structural change. Wu and Huang[(3)] conducted TL measurements using expansion chambers with different lengths, height/width ratios, thicknesses, and numbers of chambers under no-flow conditions. Chaitanya amd Munjal[(4)] studied the end corrections of the structure thickness at the entrance and exit, extending to the expansion chamber for a single expansion chamber structure with multiple resonance chambers, and used the least squares method to obtain the approximate formula of the end corrections. Selamet and Lee[(5)] studied the effect of the neck duct of the Helmholtz resonant cavity on TL when extending into the cavity and changed some fixed cross-sectional area duct extensions, expansion-form extension ducts, and perforation-form extensions. The results show that under the condition that the cavity volume remains unchanged, the resonant frequency can be changed by extending the pipe. Webster and Davies[(6)] explored the effects of cavity volume on resonance characteristics for measuring liquid and solid properties.

While conventional TL measurements typically neglect flow effects, practical mufflers operate in the presence of continuous airflow. To closely mirror actual working conditions,

recent studies have increasingly incorporated flow velocity into acoustic evaluations. Integrating computational fluid dynamics (CFD) with the finite element method (FEM) via mesh mapping, Huang *et al.*[7] used the commercial software ANSYS and COMSOL to conduct TL analysis, and proposed a one-way fluid-to-acoustic coupling method that combined CFD and acoustic FEM analysis. The TL analysis of a perforated tube muffler considering flow velocity was conducted; the results showed that the grazing flow improved the sound attenuation effect but reduced the peak resonant frequency. Kim and Selamet[8] used the wave decomposition method to measure TL, calculated the acoustic impedance of the resonant cavity from the measurement results, and observed the impact of fluid velocity on the measurement of TL. Selamet *et al.*[9] discussed the Helmholtz resonant cavity in the case where the resonant cavity was set up parallel to the pipeline path, and they considered the impact of the average flow velocity on TL. The effect of flow rate reduced the peak value of TL, but the resonance frequency changed slightly, and there was a slight downward trend. Huang *et al.*[10] studied how to reduce the frequency shift phenomenon caused by the effect of small-Mach-number flow on resonance frequency. The results showed that by modifying the pipeline structure and reducing the flow rate through the resonant cavity opening, the resonance frequency shift can be reduced. Guan *et al.*[11] modified the conventional Helmholtz resonant cavity by incorporating fixed baffles and additional necks to broaden its effective frequency range and improve sound TL performance. The pipe is changed to a curved spherical pipe. For structural variables, the effects of baffle length and height are studied, as well as the changes in TL between arc-shaped spherical connecting pipes and uniform pipes. When there is a baffle in the cavity, the resonance frequency shift will only occur when the Mach number is greater than 0.7. The arc-shaped spherical connecting tube increases the resonance frequency because the cross-sectional area of the neck of the equalizer increases.

2. Experimental Methodology and Framework

TL can be calculated by measuring the sound pressure at the inlet and outlet of the muffler, and then calculating the sound power level. In the two original measurement methods using the quadrupole parameter theory, namely, the two-sound-source method and the two-load method, shown in Figs. 1(a) and 1(b), respectively, the data should be measured twice. Note that the acoustic impedances Z_a and Z_b represent the two different acoustic termination conditions used in the conventional two-load method. The difference is that the two-sound-source method achieves different results in the measurement state by changing the input direction of the sound source, whereas the two-load method achieves different results by changing the acoustic impedance at the outlet. However, the two-sound-source method requires more time to replace equipment. In particular, when encountering more complex structures, it is necessary to consider the experimental setup methods before and after equipment replacement. The two-load rule requires attention to the difference between the two acoustic impedances. If the difference between the two is very small, it will be difficult to evaluate the muffling performance. However, there is no need to consider the method of installing the object under test after the impedance is replaced, which reduces the time and cost required for the experiment. Generally,

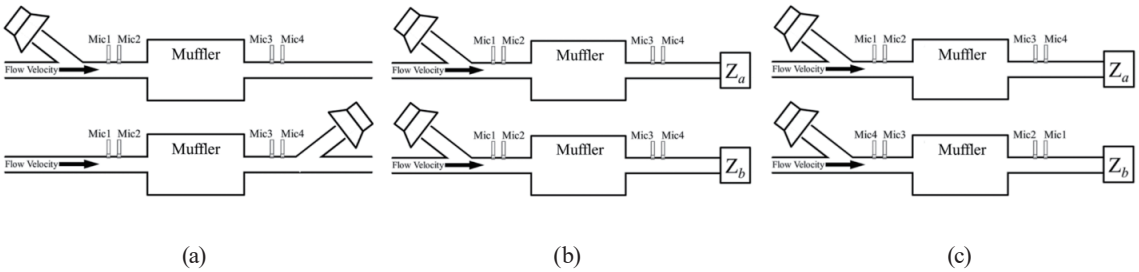


Fig. 1. Experimental setup for TL measurement using the (a) two-sound-source, (b) two-load, and (c) microphone-position-switching methods.

the measurement results of the two-sound-source method are better than those of the two-load method, but the experiment also takes more time than the two-load method.

In this study, we use the quadrupole parameter theory as the basis for measurement and developed a new measurement method called the microphone-position-switching method. Compared with the above two methods, equipment replacement takes less time than the two-sound-source method, and the improved two-load method can only produce a larger measurement difference at the outlet and has the advantages of the two-load method and does not need to consider the instrument. The disadvantage is that for asymmetric structures, the acoustic impedance at the end still needs to be changed. The entrance for this test is an extended expansion chamber. The experimental setup is shown in Fig. 1(c). The novelty of this study can be viewed in terms of a TL measurement configuration and solution strategy based on microphone-position switching, rather than as a new analytical formulation of four-pole parameters.

2.1 Four-pole parameter method

In the four-pole parameter method, the transfer matrix of a muffler is determined by measuring the sound pressures at the inlet and outlet of the muffler, as expressed in Eq. (1), followed by the calculation of the TL.

$$\boldsymbol{T} = \begin{bmatrix} T_{11} & T_{12} \\ T_{21} & T_{22} \end{bmatrix} = \begin{bmatrix} A & B \\ C & D \end{bmatrix}, \tag{1}$$

where $\boldsymbol{T}$ represents the transfer matrix, and A, B, C, and D denote the four system parameters of the four-pole model to be determined.

Because the proposed measurement method involves switching the microphone positions, a second set of measurements is required. The first set of measurements provides only two simultaneous equations, which are insufficient to determine the four parameters of the transfer matrix. Two additional simultaneous equations can be obtained by conducting the second set of measurements, resulting in a total of four simultaneous equations that are sufficient to determine the four unknown parameters.

To distinguish the state variables corresponding to the different microphone positions and instrument configurations in the subsequent equations, the measurement configurations are illustrated in Fig. 2. The subscript *I* denotes the state of the first measurement, whereas the subscript *II* denotes the state of the second measurement.

In the four-pole parameter method, the sound pressure is measured at four microphone positions. Two adjacent microphones can be used to establish a set of simultaneous equations for the transfer matrix. Therefore, the following three transfer matrices can be obtained from each measurement:

$$\begin{bmatrix} p_{1I} \\ v_{1I} \end{bmatrix} = \begin{bmatrix} A_{12} & B_{12} \\ C_{12} & D_{12} \end{bmatrix} \begin{bmatrix} p_{2I} \\ v_{2I} \end{bmatrix}, \tag{2}$$

$$\begin{bmatrix} p_{2I} \\ v_{2I} \end{bmatrix} = \begin{bmatrix} A_{23} & B_{23} \\ C_{23} & D_{23} \end{bmatrix} \begin{bmatrix} p_{3I} \\ v_{3I} \end{bmatrix}, \tag{3}$$

$$\begin{bmatrix} p_{3I} \\ v_{3I} \end{bmatrix} = \begin{bmatrix} A_{34} & B_{34} \\ C_{34} & D_{34} \end{bmatrix} \begin{bmatrix} p_{4I} \\ v_{4I} \end{bmatrix}, \tag{4}$$

where p denotes the sound pressure and v represents the particle velocity. The subscripts indicate the microphone numbers, with microphones 1 and 2 located at the inlet of the test specimen and microphones 3 and 4 located at the outlet. The subscript I denotes the measurement state. The objective is to determine the transfer matrix between microphones 2 and 3.

Because the microphones cannot directly measure particle velocity, the particle velocity must be calculated from the simultaneous equations and expressed solely in terms of the measurable sound pressure parameters. The required particle velocities v_{2I} and v_{3I} are calculated by combining the three sets of simultaneous equations. From Eq. (2), v_{2I} can be expressed in terms of the sound pressure as Eq. (5). Similarly, v_{3I} in Eq. (4) can be expressed in terms of the sound pressure as Eq. (6):

$$v_{2I} = \frac{p_{1I} - A_{12} p_{2I}}{B_{12}}, \tag{5}$$

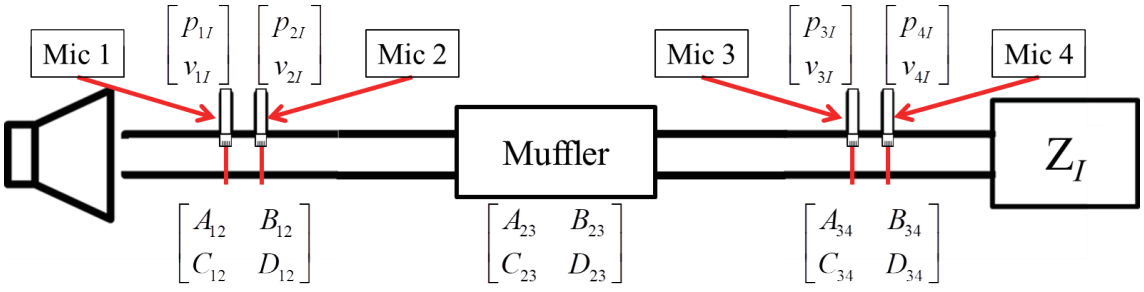


Fig. 2. (Color online) Schematic of the TL measurement setup.

$$v_{3I} = C_{34} p_{4I} + D_{34} \left(\frac{p_{3I} - A_{34} p_{4I}}{B_{34}} \right). \tag{6}$$

The parameters A_{12}, B_{12}, C_{12}, D_{12}, A_{34}, B_{34}, C_{34}, and D_{34} in the transfer matrix correspond to the measurement tubes located within the microphone fixture. Since these tubes are uniform ducts without any change in cross-sectional area, the corresponding parameters can be expressed using the analytical l formulation for a uniform duct as

$$\begin{bmatrix} A_{12} & B_{12} \\ C_{12} & D_{12} \end{bmatrix} = e^{-jMk_c l_{12}} \begin{bmatrix} \cos(k_c l_{12}) & j\frac{\rho c}{S}\sin(k_c l_{12}) \\ j\frac{S}{\rho c}\sin(k_c l_{12}) & \cos(k_c l_{12}) \end{bmatrix}, \tag{7}$$

$$\Delta_{12} = A_{12} D_{12} - B_{12} C_{12} = 1, \tag{8}$$

$$\begin{bmatrix} A_{34} & B_{34} \\ C_{34} & D_{34} \end{bmatrix} = e^{-jMk_c l_{34}} \begin{bmatrix} \cos(k_c l_{34}) & j\frac{\rho c}{S}\sin(k_c l_{34}) \\ j\frac{S}{\rho c}\sin(k_c l_{34}) & \cos(k_c l_{34}) \end{bmatrix}, \tag{9}$$

$$\Delta_{34} = A_{34} D_{34} - B_{34} C_{34} = 1, \tag{10}$$

$$k_c = \frac{k}{1 - M^2}, \tag{11}$$

where j is the imaginary unit, M is the Mach number, k_c is the convective wavenumber, ρ is the air density, and c is the speed of sound. In this study, variations in the speed of sound due to different environmental conditions are not considered; the speed of sound is fixed at 346.3 m/s. Note that this assumption is explicitly identified as a potential uncertainty source rather than being treated as an exact quantity, and it is ideally be supported by calibration data from the actual microphone, DAQ, and anemometer used in the experiment. l_{12} denotes the distance between the first and second measurement points, whereas l_{34} denotes the distance between the third and fourth measurement points. S represents the cross-sectional area of the duct, ω denotes the angular frequency, and k is the wavenumber.

The effects of mean flow on the transfer matrix can be observed by comparing Eqs. (7), (9), and (11). Because the exponential terms in Eqs. (7) and (9) contain the Mach number M, the transfer matrix T of a uniform duct under mean-flow conditions decreases to the corresponding transfer matrix under no-flow conditions when $M = 0$, and Eq. (11) then decreases to the result that the convective wavenumber k_c, which is affected by the mean flow, becomes equal to the wavenumber k.

Using the sound-pressure expressions for v_{2I} and v_{3I} obtained from Eqs. (5) and (6), respectively, we can rewrite Eq. (3) as Eq. (12).

$$\begin{bmatrix} p_{2I} \\ \dfrac{p_{1I} - A_{12}p_{2I}}{B_{12}} \end{bmatrix} = \begin{bmatrix} A_{23} & B_{23} \\ C_{23} & D_{23} \end{bmatrix} \begin{bmatrix} p_{3I} \\ C_{34}p_{4I} + D_{34}\left(\dfrac{p_{3I} - A_{34}p_{4I}}{B_{34}} \right) \end{bmatrix} \tag{12}$$

Equation (12) represents the simultaneous equations obtained from the first measurement. Because the two simultaneous equations are insufficient to determine the four unknown parameters, a second measurement was performed to obtain two additional simultaneous equations. Following the same derivation procedure described in Eqs. (2)–(6), the simultaneous equations for the second measurement can be derived as

$$\begin{bmatrix} p_{3II} \\ \dfrac{p_{4II} - A_{12}p_{3II}}{B_{12}} \end{bmatrix} = \begin{bmatrix} A_{23} & B_{23} \\ C_{23} & D_{23} \end{bmatrix} \begin{bmatrix} p_{2II} \\ C_{34}p_{1II} + D_{34}\left(\dfrac{p_{2II} - A_{34}p_{1II}}{B_{34}} \right) \end{bmatrix}. \tag{13}$$

Equations (12) and (13) provide four simultaneous equations, from which the frequency response function (FRF) can be calculated as

$$\frac{p_{iI}}{p_{jI}} = H_{ijI}, \tag{14}$$

where i and j denote the microphone numbers. After calculating the FRF, Eqs. (12) and (13) can be rewritten as Eqs. (15) and (16), respectively.

$$\begin{bmatrix} H_{23I} \\ \dfrac{H_{13I} - A_{12}H_{23I}}{B_{12}} \end{bmatrix} = \begin{bmatrix} A_{23} & B_{23} \\ C_{23} & D_{23} \end{bmatrix} \begin{bmatrix} H_{33I} \\ C_{34}H_{43I} + D_{34}\left(\dfrac{1 - A_{34}H_{43I}}{B_{34}} \right) \end{bmatrix} \tag{15}$$

$$\begin{bmatrix} H_{32II} \\ \dfrac{H_{42II} - A_{12}H_{32II}}{B_{12}} \end{bmatrix} = \begin{bmatrix} A_{23} & B_{23} \\ C_{23} & D_{23} \end{bmatrix} \begin{bmatrix} H_{22II} \\ C_{34}H_{12II} + D_{34}\left(\dfrac{1 - A_{34}H_{12II}}{B_{34}} \right) \end{bmatrix} \tag{16}$$

By solving the four simultaneous equations given by Eqs. (15) and (16), we can obtain the four unknown system parameters of the transfer matrix $\boldsymbol{T}$ as follows.

$$A_{23} = \frac{\Delta_{34}\left(H_{23I}H_{43II} - H_{23II}H_{43I}\right) + D_{34}\left(H_{23II} - H_{23I}\right)}{\Delta_{34}\left(H_{43II} - H_{43I}\right)} \tag{17}$$

$$B_{23} = \frac{B_{34}\left(H_{23I} - H_{23II}\right)}{\Delta_{34}\left(H_{43II} - H_{43I}\right)} \tag{18}$$

$$C_{23} = \frac{\left(H_{13I} - A_{12}H_{23I}\right)\left(\Delta_{34}H_{12II} - D_{34}\right) - \left(H_{42II} - A_{12}H_{32II}\right)\left(\Delta_{34}H_{43I} - D_{34}\right)}{B_{12}\Delta_{34}\left(H_{12II} - H_{43I}\right)} \tag{19}$$

$$D_{23} = \frac{B_{34}\left(H_{13I} - H_{13II}\right) + A_{12}\left(H_{23II} - H_{23I}\right)}{B_{12}\Delta_{34}\left(H_{43II} - H_{43I}\right)} \tag{20}$$

The sound pressure data measured by the microphones are processed using Eqs. (17)–(20) and then substituted into the TL equation, as given in Eq. (21), thereby completing the TL performance measurement of the muffler.

$$TL\left(\omega i\right) = 20\log_{10}\left(\frac{1}{2}\frac{1+M_i}{1+M_o}\left|A_{23}\left(\omega i\right) + \frac{B_{23}\left(\omega i\right)}{\rho c} + \rho c C_{23}\left(\omega i\right) + D_{23}\left(\omega i\right)\right|\right), \tag{21}$$

where TL represents the TL, M_i denotes the Mach number at the inlet, and M_o denotes the Mach number at the outlet. The TL equation also reflects the difference between no-flow and mean-flow conditions. For measurements under no-flow conditions, the Mach number terms can be neglected.

The theoretical basis of the TL measurement is established under the assumptions of plane-wave propagation, incompressible flow, and a nonviscous medium. However, fluid flow is driven by pressure differences within the flow field, and gases can undergo density variations as the pressure changes. When the density variation becomes significant, the flow should be treated as compressible, which deviates from the assumptions underlying the conventional TL measurement theory. According to fluid mechanics theory,[12] when the Mach number is less than 0.3 ($M < 0.3$), the flow can generally be approximated as incompressible. Therefore, the mean-flow conditions considered in this study remain within the applicable range of theoretical assumptions for TL measurement.

2.2 Effects of experimental equipment on measurement results

The measurement system used in this study consisted of measurement microphones, a data acquisition (DAQ) card (NI 9234) for acquiring measurement signals, an anemometer, a loudspeaker, a power amplifier, a blower, a manifold, a microphone fixture, connecting ducts, a simple expansion chamber, and an inlet-extended expansion chamber. LabVIEW was used to develop the TL measurement algorithms, whereas COMSOL Multiphysics was employed for the finite element analysis (FEA) of TL under mean-flow conditions.

2.2.1 Microphone spacing

According to the literature, the microphone spacing imposes measurement limitations associated with the acoustic wavelength.[2] The microphone spacing should be greater than 1% of the wavelength corresponding to the lowest frequency of interest and less than one-half of the wavelength corresponding to the highest frequency of interest, as expressed in Eq. (22). In addition, the literature recommends that the microphone spacing in the high-frequency range be approximately 80% of the wavelength corresponding to the highest frequency of interest.

$$\frac{0.01c}{f_l} < b < \frac{c}{2f_u} \times 80\%, \tag{22}$$

where b denotes the microphone spacing, f_l represents the lower measurement frequency limit, and f_u represents the upper measurement frequency limit. Because these two spacing requirements cannot be simultaneously satisfied over the entire frequency range, two microphone fixtures with different microphone spacings were employed in this study. The microphone spacings were 300 and 30 mm. On the basis of Eq. (22), the applicable frequency range for the microphone fixture with a spacing of 300 mm is 11.54–461.73 Hz, whereas that for the microphone fixture with a spacing of 30 mm is 115.43–4617.33 Hz. Accordingly, different microphone fixtures were selected for the experiments depending on the frequency range of interest.

2.2.2 FRF correction procedure

The FRF is defined as the complex ratio of the output signal to the input signal. In the measurement system, discrepancies in the amplitude and phase response of the microphones may affect the measurement accuracy. Therefore, the correction method proposed for the two-microphone transfer function method[13] was adopted in this study to reduce measurement errors in the FRF.

First, the FRF was measured using the initial microphone configuration. The sound pressure signals measured by the microphones were used to calculate the FRF according to Eq. (14). The microphone positions were then switched, and a second FRF measurement was performed, as illustrated in Fig. 3.

The FRFs obtained from the first and second measurements were substituted into Eq. (23) to calculate the correction function for the frequency response:

$$H_c = \sqrt{H_I \times H_{II}}, \tag{23}$$

where H_c denotes the correction function, H_I represents the FRF obtained from the first measurement, and H_{II} represents the FRF obtained from the second measurement.

The correction function was then used to normalize the FRF and correct its phase response, thereby reducing measurement errors caused by discrepancies in amplitude and phase between the microphones.

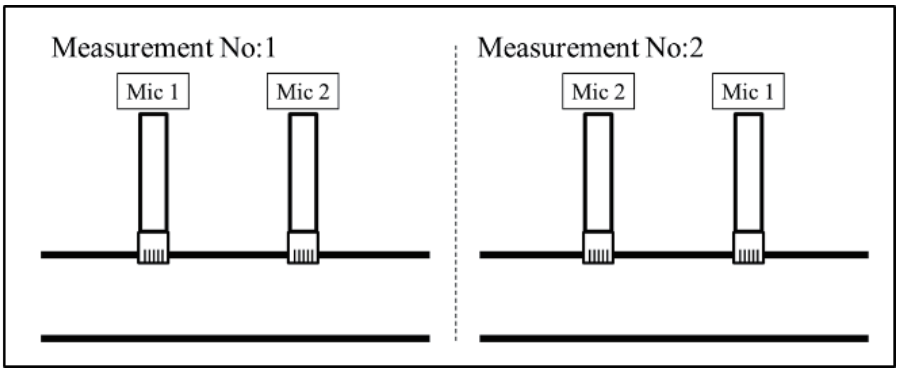


Fig. 3. Schematic of the FRF correction procedure.

Because the calculation of the correction function can be regarded as a geometric mean, the arithmetic–geometric mean inequality was considered in this study. When the condition $H_I = H_{II}$ is satisfied, the arithmetic mean is equal to the geometric mean. However, the experimental results showed that the geometric-mean correction produced notable signal uncertainty in TL measurements under mean-flow conditions. Therefore, the arithmetic mean was also investigated as an alternative correction approach for the FRF to reduce configuration-dependent experimental uncertainty and provide an alternative means of generating independent measurement equations.

2.3 FEA

To investigate TL characteristics under mean-flow conditions, COMSOL Multiphysics was employed for FEA. The TL under both no-flow and mean-flow conditions was simulated and compared with analytical solutions and experimental results to verify the consistency and reliability of the numerical predictions. For the simulation of TL under mean-flow conditions, acoustic analysis alone is insufficient; therefore, a coupled flow–acoustic analysis was required. First, CFD analysis was performed to obtain the steady-state flow field distribution. The calculated flow field was then coupled with the acoustic model and used as the initial condition for the subsequent acoustic analysis. In this study, the shear stress transport (SST) turbulence model was adopted for the CFD simulation to characterize the mean-flow behavior, whereas the linearized Navier–Stokes equations were applied for the acoustic analysis. After completing the coupled flow–acoustic simulation, the numerical results were compared with theoretical predictions and experimental measurements to evaluate the effects of mean flow on TL characteristics and to confirm the validity of the proposed simulation approach.

3. Results and Discussion

Since in this paper, we propose a microphone-position-switching method for TL measurement, the two-load method was first employed to measure the TL as a reference. This approach was used as a preliminary validation procedure to evaluate the reliability and accuracy of the proposed measurement results.

3.1 Simple expansion chamber

The TL measurement under no-flow conditions was first conducted in this study. The TL was calculated using two algorithms, namely, the two-load method and the microphone-position-switching method, as shown in Fig. 4. Subsequently, correction functions were incorporated into the algorithms, resulting in five different calculation approaches, as presented in Fig. 5. The results indicate that the TL curves obtained using the two-load and microphone-position-switching methods exhibited nearly identical trends. To reduce measurement errors, correction functions were introduced. In this study, two types of correction function were investigated: the arithmetic mean and the geometric mean. As shown in Fig. 5, the incorporation of correction functions reduced the deviation between the corrected results and the results obtained using the original algorithms. A comparison of the results further demonstrates that the microphone-position-switching method exhibited a similar trend to the two-load method. This agreement confirms that the proposed algorithm is capable of providing reliable TL measurements. Furthermore, the application of correction functions effectively reduces the measurement errors associated with the original algorithms. Note that the proposed microphone-position-switching method inherently requires two measurement states. Therefore, the consistency between the two states is particularly important for assessing the robustness of the method. However, the agreement between the microphone-position-switching method and the two-load method should be interpreted as method validation, whereas repeated measurements are required to establish measurement repeatability in the future work.

The differences between the experimental measurements and numerical simulation results are compared in Fig. 6. The results show good agreement in terms of the overall TL trends. However, significant deviations between the analytical solution and the experimental and numerical results were observed above approximately 2000 Hz. This discrepancy is attributed to the analytical formulation adopted in this study, which is based on a one-dimensional transfer matrix method under the assumption of plane-wave propagation. When the acoustic field can no

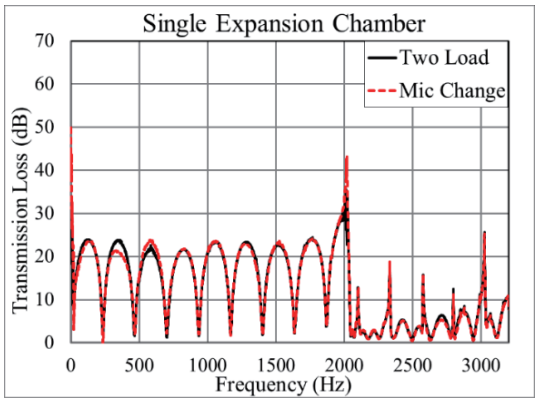


Fig. 4. (Color online) Measured TL of a simple expansion chamber under no-flow conditions.

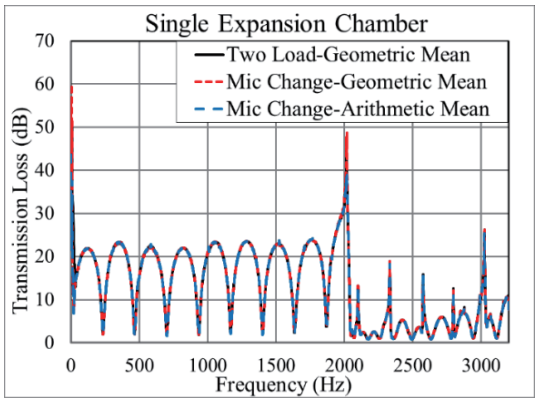


Fig. 5. (Color online) Measured TL of a simple expansion chamber with the correction function under no-flow conditions.

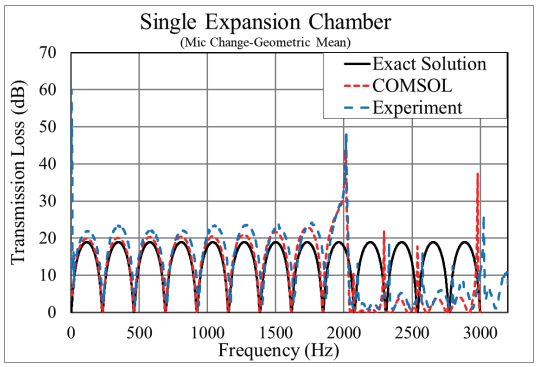


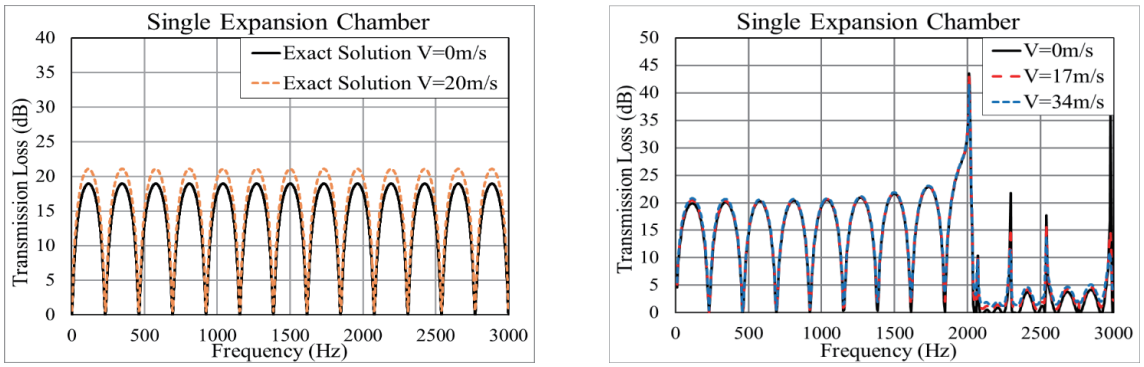
Fig. 6. (Color online) Comparison of TL measurements of a simple expansion chamber under no-flow conditions.

longer be approximated as one-dimensional, the analytical solution becomes unsuitable. The cutoff frequency represents the condition at which acoustic propagation can no longer be described as a plane wave. As the measurement frequency approaches the cutoff frequency, the discrepancy between the analytical solution and the experimental or numerical results increases, indicating a reduction in the reliability of the theoretical prediction.

The validation of the simple expansion chamber under no-flow conditions confirmed the reliability of the proposed measurement algorithms, enabling further investigation under mean-flow conditions. The effects of mean flow were first analyzed using both the analytical solution and FEA, as shown in Fig. 7. The results indicate that considering mean flow increased the TL compared with the no-flow condition. In addition, no significant shift in resonance frequency was observed owing to the effect of mean flow.

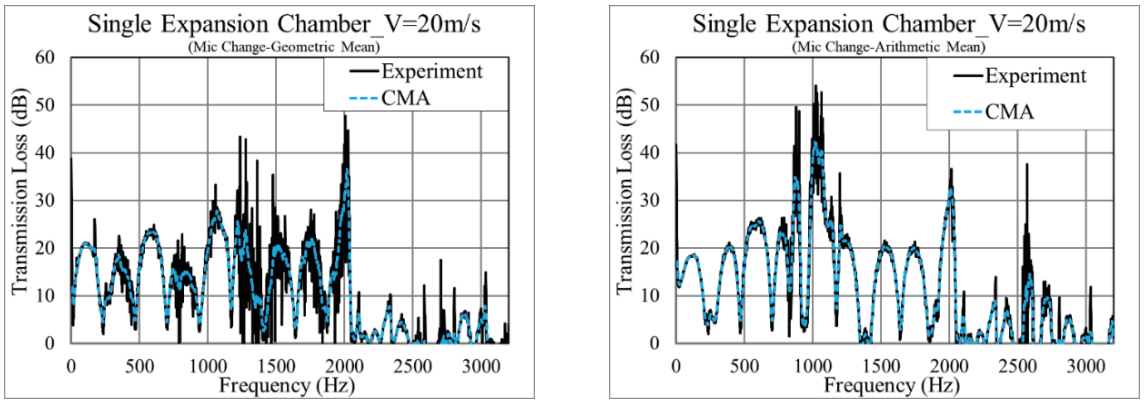
The experimental results were subsequently analyzed. During the measurements, short-term signal uncertainty was observed. Therefore, a centered moving average (CMA) was applied to suppress short-term fluctuations and smooth TL curves, as shown in Fig. 8. The results indicate that the measurement data corrected using the arithmetic mean exhibited fewer fluctuations than those corrected using the geometric mean. However, significant differences were observed between the two correction methods in terms of the calculated TL results. Figures 9 and 10 show the TL results obtained using different algorithms. It can be observed that the application of the correction function significantly affected the calculated TL characteristics. The results obtained using the arithmetic mean as the correction function were similar to those obtained without correction, whereas the algorithms employing the geometric mean correction exhibited more consistent TL results.

The deviation between the experimental measurements and numerical simulations is shown in Fig. 11. Similar to the no-flow condition, the reliability of the calculated results decreased above approximately 2000 Hz owing to the limitations of the one-dimensional transfer matrix method beyond the cutoff frequency. Nevertheless, the overall trends of the analytical solution and numerical analysis results were in good agreement. According to the simulation results, mean flow was expected to enhance the TL performance. Therefore, the experimental results under mean-flow conditions were further compared with those under no-flow conditions, as shown in Fig. 12. The comparison indicates that the improvement in TL caused by mean flow



(a) (b)

Fig. 7. (Color online) Analytical and numerical TL results of a simple expansion chamber under mean-flow conditions. (a) Transfer matrix method and (b) FEA.



(a) (b)

Fig. 8. (Color online) Calculation of TL using the CMA with (a) geometric and (b) arithmetic means for a simple expansion chamber.

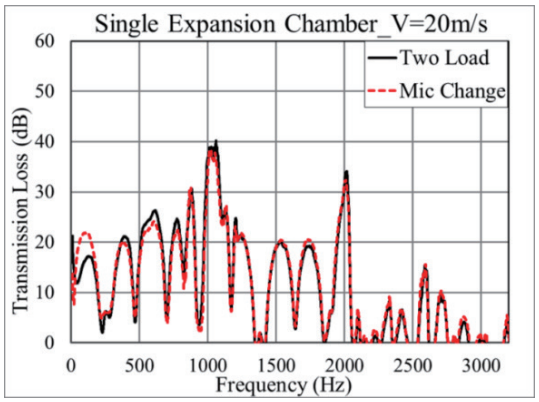


Fig. 9. (Color online) Measured TL under mean-flow conditions for a simple expansion chamber.

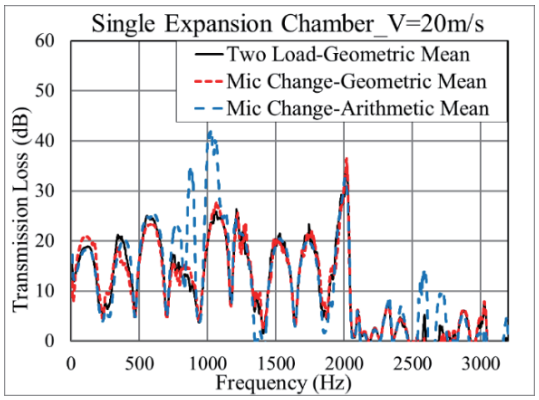


Fig. 10. (Color online) Measured TL with the correction function under mean-flow conditions for a simple expansion chamber.

was difficult to clearly identify from the experimental data. However, from the overall trend of the TL curve, the characteristic behavior of the simple expansion chamber under mean-flow conditions could still be identified.

3.2 Inlet-extended expansion chamber

The inlet-extended expansion chamber, which introduces additional duct variation compared with the simple expansion chamber, was further investigated. The TL was first measured under no-flow conditions, the results of which are shown in Figs. 13 and 14. Similarly to the results obtained for the simple expansion chamber, the TL deviations between the two-load and microphone-position-switching methods decreased after applying the correction function. The experimental results were subsequently compared with the analytical solution and FEA results, as shown in Fig. 15. Overall, the experimental measurements, analytical predictions, and numerical simulations exhibited similar TL trends. However, notable discrepancies were observed near the cutoff frequencies of 500 and 1955 Hz. These deviations are considered to be caused by manufacturing imperfections of the test specimen. Owing to the dimensional limitations of the 3D printing process, the specimen had to be fabricated as two separate components and subsequently assembled manually. Imperfections at the bonding interface may have altered the wall geometry and affected the measured TL characteristics.

The validation under no-flow conditions for the inlet-extended expansion chamber demonstrated good agreement among the experimental results, analytical solutions, and numerical simulations, further confirming the reliability of the proposed measurement algorithms. Subsequently, TL under mean-flow conditions was investigated using both analytical solutions and FEA to evaluate the effect of flow, as shown in Fig. 16. The results indicate that considering mean flow generally enhanced the TL performance. However, the TL at approximately 400, 1220, and 1940 Hz decreased under mean-flow conditions. This phenomenon is attributed to the structural difference between the inlet-extended and simple expansion chambers. The extended duct section introduces a quarter-wavelength resonator effect, and the

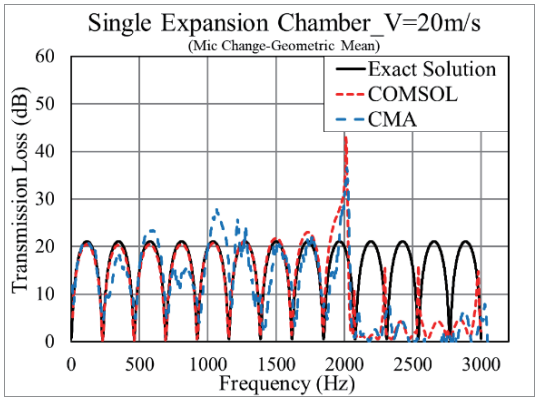


Fig. 11. (Color online) Comparison of TL measurements under mean-flow conditions for a simple expansion chamber.

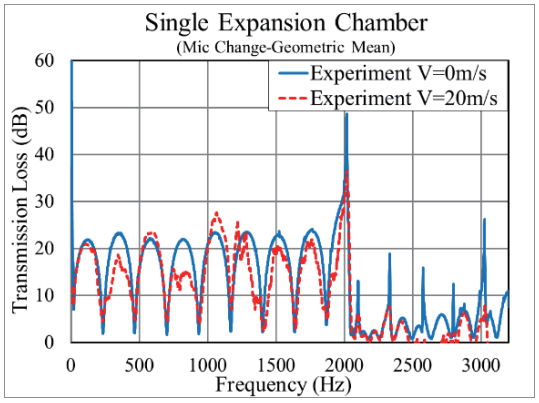


Fig. 12. (Color online) Comparison of TL measurements under mean-flow and no-flow conditions for a simple expansion chamber.

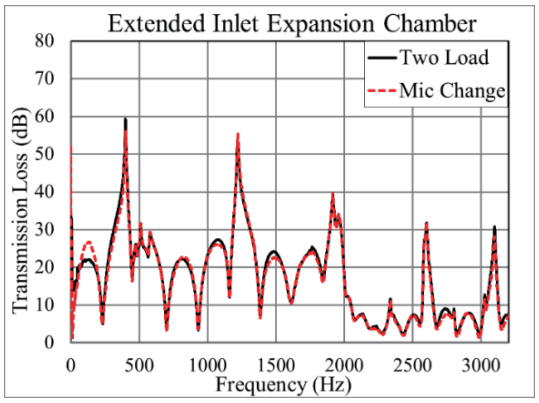


Fig. 13. (Color online) Measured TL of an inlet-extended expansion chamber under no-flow conditions.

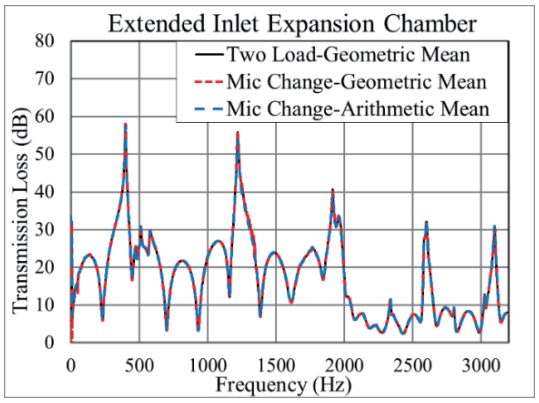


Fig. 14. (Color online) Measured TL of an inlet-extended expansion chamber with the correction function under no-flow conditions.

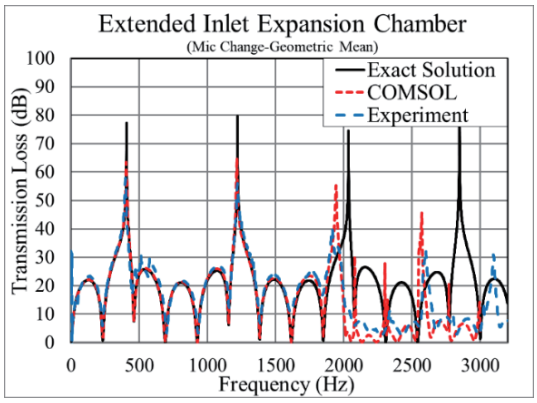
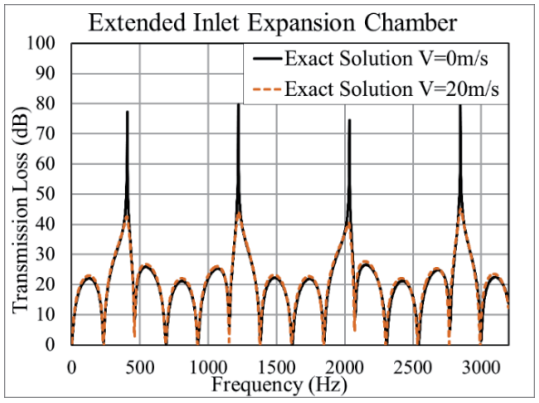
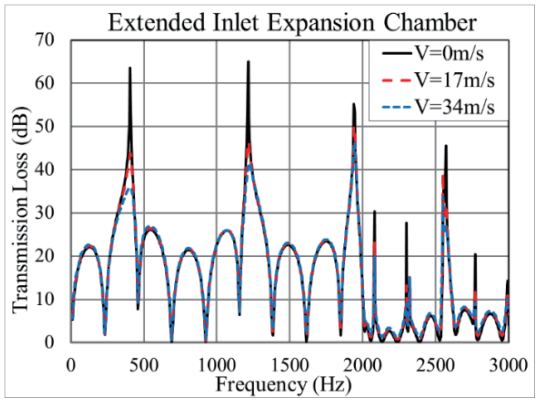


Fig. 15. (Color online) Comparison of TL measurements of an inlet-extended expansion chamber under no-flow conditions.



(a)



(b)

Fig. 16. (Color online) Analytical and numerical TL results of an inlet-extended expansion chamber under mean-flow conditions. (a) Transfer matrix method and (b) FEA.

increase in mean flow causes a reduction in TL at the corresponding resonance frequencies. In addition, similar to the simple expansion chamber, the cutoff frequency effect also affects the prediction accuracy, resulting in significant deviations between the analytical solution and FEA results near 1900 Hz.

After analyzing the effect of mean flow using the analytical solution and FEA, experimental measurements were conducted. A CMA was applied to suppress short-term signal fluctuations, as shown in Fig. 17. Similarly to the results obtained for the simple expansion chamber, the measurement data corrected using the arithmetic mean exhibited fewer fluctuations than those corrected using the geometric mean. The TL results calculated using different algorithms and correction functions are presented in Figs. 18 and 19. The results show that the calculated curves exhibited two different trends near 950 Hz. One trend was observed for the two-load, microphone-position-switching, and arithmetic mean correction methods, whereas the other trend was obtained using the geometric mean correction method. The TL obtained using the geometric mean correction showed better agreement with the analytical and simulation results. Therefore, the geometric mean correction was considered more appropriate for the proposed measurement algorithm.

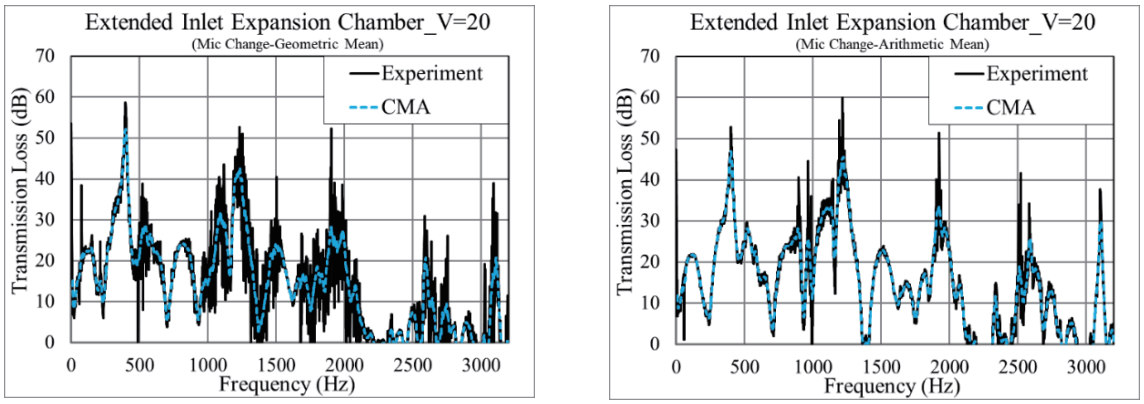
The comparison between the experimental and numerical simulation results is shown in Fig. 20. At around 950 Hz, both the analytical solution and FEA results exhibited trends similar to those obtained using the geometric mean correction. This indicates that the geometric-mean correction provides more reliable TL predictions. Overall, the experimental, analytical, and numerical results showed consistent trends, demonstrating the validity of the proposed measurement and numerical models.

Finally, the effect of mean flow on the TL performance was investigated, as shown in Fig. 21. The results indicate that the TL characteristics under mean-flow conditions were generally similar to those under no-flow conditions, except near the quarter-wavelength resonator frequency. The resonance frequency of the resonator shifted toward lower values under mean-flow conditions, which is consistent with the expected effect of flow. The good agreement between the experimental and numerical results confirms the validity of the proposed analysis approach.

3.3 Helmholtz resonator

The TL performance of the Helmholtz resonator was further verified. The measured TL under no-flow conditions is shown in Fig. 22. The results indicate that the TL curves calculated using different algorithms exhibited similar trends. As observed for the other test specimens, the incorporation of the correction function effectively reduced the deviation between the proposed and original calculation methods.

The experimental results were further compared with the numerical simulation results. The measured resonance frequency was 84 Hz, which is slightly different from the analytical solution of 89 Hz and the FEA result of 88 Hz. In addition, an unexpected TL peak was observed at approximately 230 Hz. This phenomenon is presumed to be caused by structural imperfections in the test specimen. The Helmholtz resonator investigated in this study was fabricated using a 3D printer. Owing to the dimensional limitations of the 3D printing process, the resonator had to be manufactured as multiple components and subsequently assembled. The defects generated



(a) (b)

Fig. 17. (Color online) Calculation of TL using the CMA with (a) geometric and (b) arithmetic means for an inlet-extended expansion chamber.

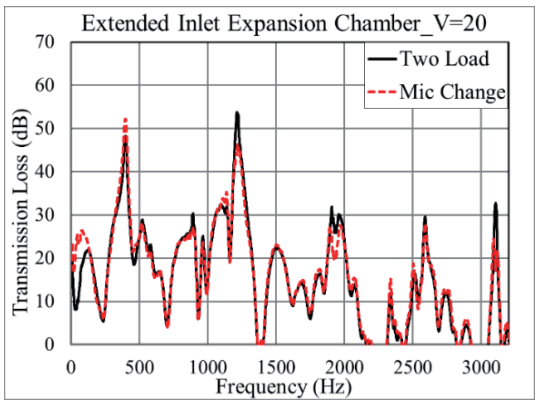


Fig. 18. (Color online) Measured TL under mean-flow conditions for an inlet-extended expansion chamber.

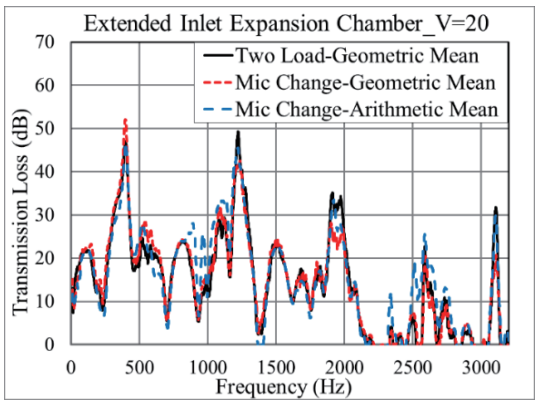


Fig. 19. (Color online) Measured TL with the correction function under mean-flow conditions for an inlet-extended expansion chamber.

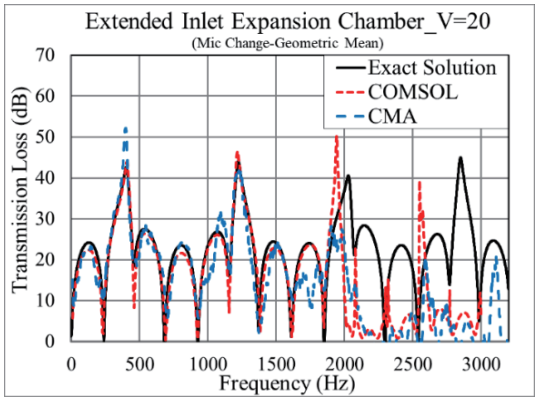


Fig. 20. (Color online) Comparison of TL measurements under mean-flow conditions for an inlet-extended expansion chamber.

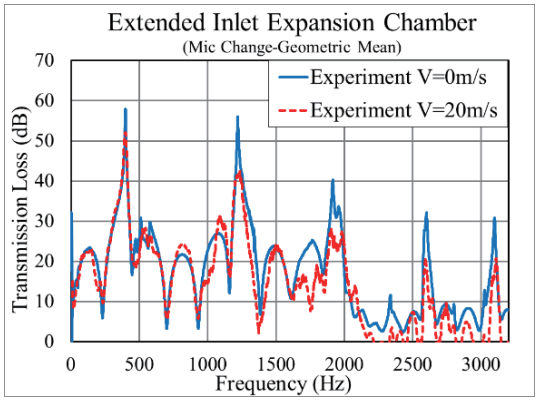


Fig. 21. (Color online) Comparison of TL measurements under mean-flow and no-flow conditions for an inlet-extended expansion chamber.

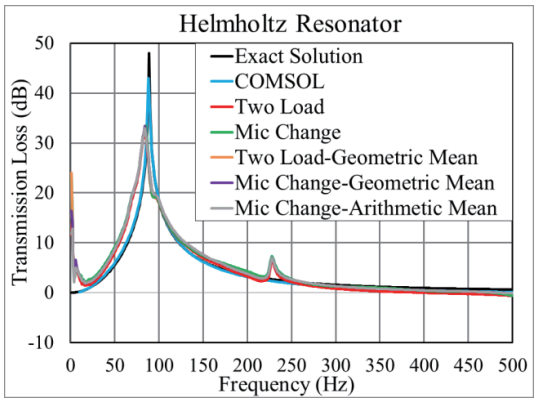


Fig. 22. (Color online) Calculated TL of a Helmholtz resonator under no-flow conditions.

during the assembly process may have altered the acoustic characteristics and affected the measurement results. Furthermore, a difference of more than 10 dB was observed between the experimental and simulation results in terms of TL magnitude. This discrepancy is attributed to the fact that air damping effects were not considered in the analytical and numerical calculations, resulting in an overestimation of the TL performance. According to Fig. 23[14] and Eq. (24), the predicted TL of the Helmholtz resonator was estimated to be approximately 26–36 dB. The experimental value of 33.34 dB falls within this predicted range, confirming the validity of the analytical estimation and numerical analysis.

$$K = \frac{\sqrt{S_n V_c / l_{eq}}}{2S}, \tag{24}$$

where S_n represents the neck area of the Helmholtz resonator, V_c denotes the cavity volume, l_{eq} is the corrected neck length, S represents the cross-sectional area of the duct, and K is the ratio of frequency to TL.

The TL measurement under mean-flow conditions was subsequently performed. A CMA was applied to suppress short-term signal fluctuations, as shown in Fig. 24. Similarly to the results obtained for the other test specimens, the measurement data corrected using the arithmetic mean exhibited fewer fluctuations than those corrected using the geometric mean. The measurement results showed that different algorithms exhibited similar TL trends. However, two resonance peaks were observed in the experimental results, corresponding to approximately 80 and 96 Hz, as shown in Fig. 25. To resolve the occurrence of two resonance frequencies in the measured data, the expected frequency method was introduced in this study.[15] This method was used to determine the representative characteristic frequency of a random signal within a specified narrow frequency band. The method applies only to random signal measurements, and the frequency range used for calculation must be predefined. The calculation equation is expressed as

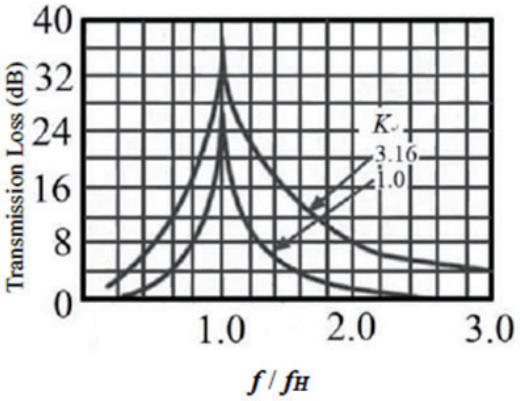
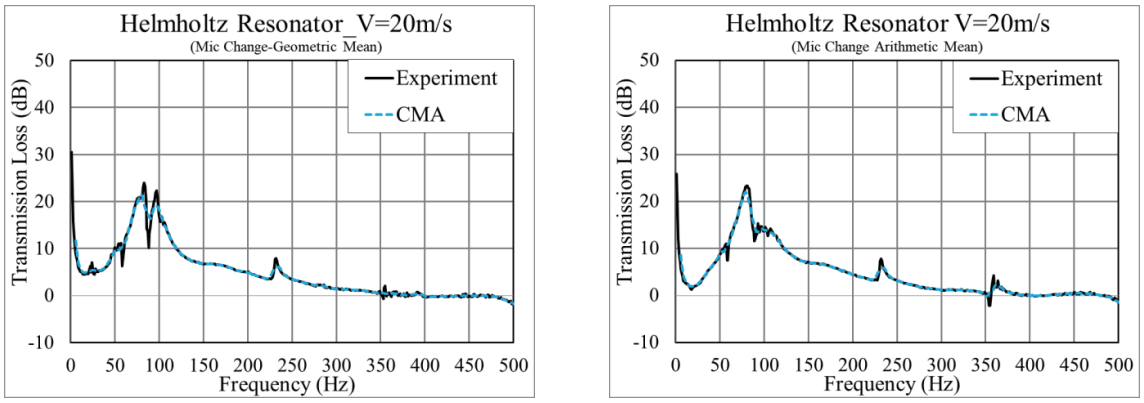


Fig. 23. TL of a Helmholtz resonator.[14]



(a) (b)

Fig. 24. (Color online) Calculation of TL using the CMA with (a) geometric and (b) arithmetic means for a Helmholtz resonator.

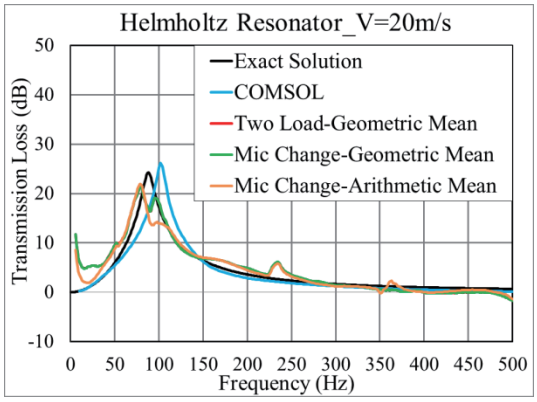


Fig. 25. (Color online) TL measurement of a Helmholtz resonator under mean-flow conditions.

$$\omega_0^2 = \frac{\int_{-\infty}^{\infty} \omega^2 S_w(\omega) d\omega}{\int_{-\infty}^{\infty} S_w(\omega) d\omega}, \tag{25}$$

where ω_0 represents the expected frequency, ω denotes the angular frequency, and S_w is the weighting function. In this study, the weighting function is defined as the magnitude of TL. According to the literature, the expected frequency is defined as the weighted average of the angular frequency within a specified narrow frequency bandwidth. The following three methods were employed to determine the frequency bandwidth: the statistical quartile method, the octave band method, and the one-third octave band method, which are commonly used in acoustic analysis. The frequency bandwidths obtained using these three methods are summarized in Table 1. Since the expected frequencies calculated from all three bandwidth definitions were concentrated near 96 Hz, the resonance frequency of the experimental measurement was identified as approximately 96 Hz.

The TL results under mean-flow conditions were further compared with the analytical and numerical predictions, as shown in Fig. 26. The experimental resonance frequency was approximately 96 Hz, whereas the analytical solution and FEA predicted resonance frequencies of 90 and 102 Hz, respectively. Since the analytical solution was derived on the basis of experimental parameters, the deviation is considered to originate from uncertainties in the original measurement data, which subsequently affected the analytical calculation. The discrepancy between the experimental and FEA results is mainly attributed to imperfections in

Table 1
Expected frequencies calculated using different narrow-band definitions for a Helmholtz resonator.

Narrow-band calculation method	Expected frequency (Hz)	Frequency bandwidth
Experimental	80	—
	96	—
Quartile	91.89	11.54 Hz–152.95 Hz
Octave band	91.78	63 Hz–125 Hz
One-third octave band	90.18	70.8 Hz–112 Hz

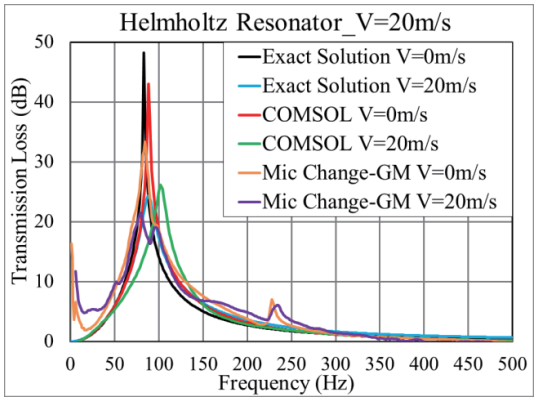


Fig. 26. (Color online) Comparison of the effects of mean flow on TL for a Helmholtz resonator.

the fabricated resonator structure. The no-flow measurement results already exhibited a slight deviation in resonance frequency; therefore, similar deviations were expected when the mean-flow effect was introduced. Regarding the TL magnitude, the difference between the experimental and predicted results was approximately 6 dB. The experimental TL was slightly lower than the analytical and numerical results, which is attributed to the damping effect of air that was not fully considered in the analytical and numerical models.

After completing the TL validation, the effect of mean flow on the Helmholtz resonator was confirmed experimentally. The results revealed a clear reduction in TL performance and a shift in resonance frequency toward higher values. These trends were consistent with both the analytical solution and numerical simulation results. Through the validation of the TL characteristics of the simple expansion chamber, inlet-extended expansion chamber, and Helmholtz resonator, we confirmed that the experimental measurements, analytical predictions, and numerical simulations exhibited similar trends. Therefore, the proposed measurement algorithms and FEA model were demonstrated to have satisfactory validity for evaluating TL characteristics.

3.4 Automotive-muffler assembly

The proposed TL measurement method was further applied to evaluate the acoustic performance of a commercially available automotive-muffler assembly, as shown in Fig. 27. According to the manufacturer's specifications, the automotive-muffler assembly incorporates four Helmholtz resonators with resonance frequencies of 90, 230, 285, and 410 Hz. The TL was first measured under no-flow conditions and compared with the manufacturer's specification curve. Since the original numerical data were unavailable, the measurement results were superimposed on the manufacturer's specification curve for comparison, as shown in Fig. 28. The measured TL exceeded the specification curve at the resonance frequencies corresponding to most resonators. However, the TL at the nominal resonance frequency of 230 Hz did not



Fig. 27. (Color online) Experimental setup for the automotive-muffler assembly.

satisfy the specified performance. Further experimental verification revealed that the actual resonance frequency of this resonator was approximately 290 Hz, as illustrated in Fig. 29, explaining the discrepancy between the measurement and specified results.

TL measurements were subsequently performed under mean-flow conditions. A CMA was applied to suppress short-term signal fluctuations, and the processed results are presented in Fig. 30. The correction function based on the arithmetic mean produced smoother TL curves than that based on the geometric mean. The TLs calculated using different algorithms are compared in Figs. 31 and 32. The results indicate that the arithmetic mean correction yielded TL curves that were more similar to those obtained using the original two-load and microphone-position-switching methods. In contrast, the algorithms employing the geometric mean correction produced consistent TL results with each other. On the basis of the verification results, the incorporation of a correction function is essential for obtaining reliable TL measurements. Although the arithmetic mean correction provides smoother measurement curves, the geometric mean correction demonstrates superior consistency with the validated TL

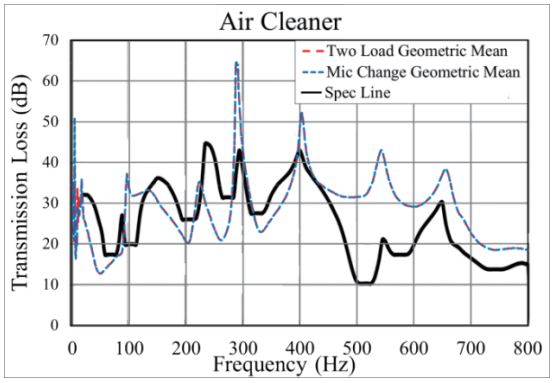


Fig. 28. (Color online) Measured TL of the automotive-muffler assembly under no-flow conditions.

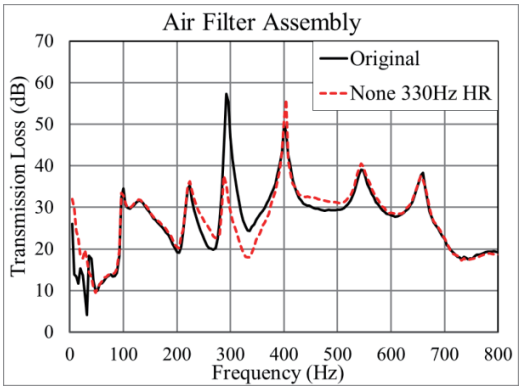
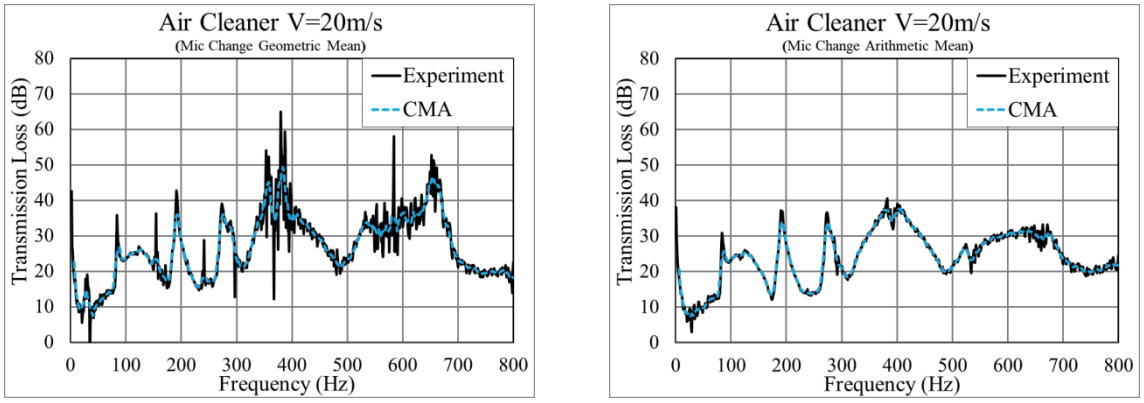


Fig. 29. (Color online) Validation of transmission loss performance for the resonator integrated into the automotive-muffler assembly.



(a) (b)

Fig. 30. (Color online) TLs caluculated using the CMA with (a) geometric and (b) arithmetic means for the automotive-muffler assembly.

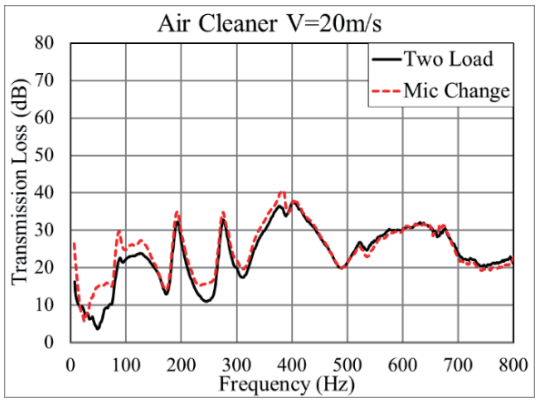


Fig. 31. (Color online) Measured TL of the automotive-muffler assembly under mean-flow conditions.

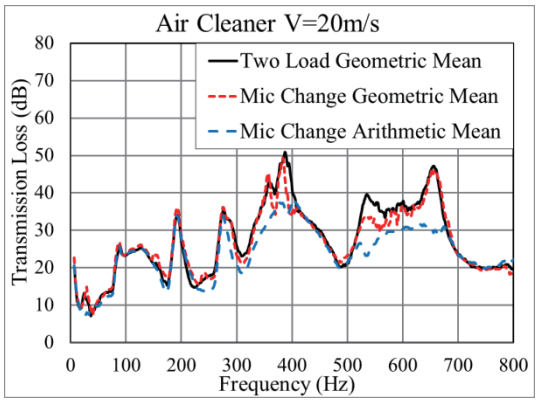


Fig. 32. (Color online) Measured TL with the correction function under mean-flow conditions for the automotive-muffler assembly.

characteristics. Therefore, the geometric mean is considered a more appropriate correction function for the proposed TL measurement algorithm.

On the basis of the manufacturer's specifications and TL measurements under no-flow conditions, the automotive-muffler assembly was found to contain four resonant chambers. According to the verification results obtained from the simplified resonator models, the presence of mean flow was expected to reduce the TL and shift the resonance frequencies toward higher values. However, the experimental results for the automotive-muffler assembly only partially agreed with these predictions. As shown in Fig. 33, the resonance frequency at 295 Hz shifted to approximately 350 Hz under mean-flow conditions, accompanied by a TL reduction of approximately 20 dB, which was consistent with the expected trend. In contrast, the resonance at 90 Hz exhibited only a decrease in TL without an obvious frequency shift. This discrepancy is attributed to the installation orientation of the resonant chamber within the duct system. Because the opening of the resonant chamber was aligned parallel to the flow direction,[10] rather than perpendicular as in the verification model, the effect of mean flow differed, as illustrated in Fig. 34. FEA was subsequently performed to further investigate the flow effects. The simulation results indicated that, under mean-flow conditions, the resonance frequencies shifted toward lower values rather than higher values, as shown in Fig. 35. A similar low-frequency shift was also observed in the experimental measurements of the automotive-muffler assembly, demonstrating good agreement between the numerical and experimental results. Furthermore, the resonance frequencies of 230 and 410 Hz also deviated from the predicted behavior. This difference is mainly attributed to the square duct geometry of the automotive-muffler assembly, which differs from the simplified resonator configuration adopted in the validation study. Previous studies have shown that the duct geometry can affect the internal flow field, thereby affecting the TL characteristics.[11] In addition, the interaction between mean flow and resonators differs between circular and square ducts, resulting in different TL behaviors and resonance frequency shifts.[12] In some cases, no significant frequency shift or TL degradation is

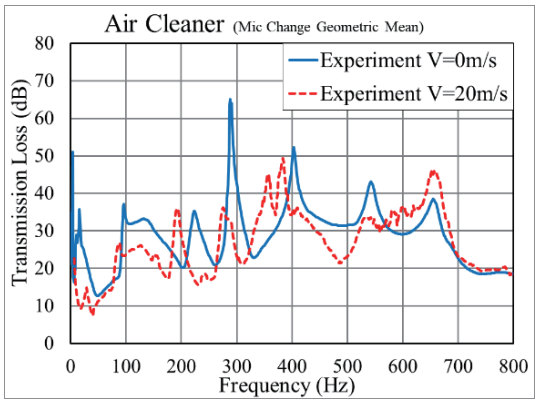


Fig. 33. (Color online) Comparison of the effect of flow velocity on the transmission loss of the automotive-muffler assembly.

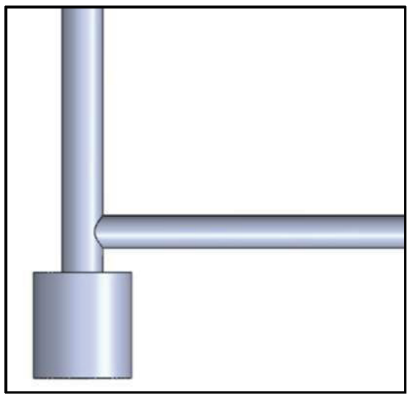


Fig. 34. (Color online) Schematic of the resonator setup installed parallel to the flow direction.

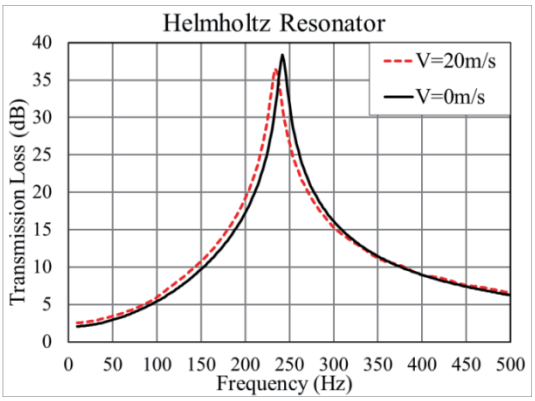


Fig. 35. (Color online) FEA results for the resonator aligned parallel to the flow direction.

observed. To further verify these effects, the finite element model was modified to include a simplified square duct with a Helmholtz resonator located near a duct bend, as shown in Fig. 36. The simulation results, presented in Fig. 37, revealed that the effect of mean flow on the Helmholtz resonator differed substantially from the theoretical expectation. Specifically, the resonance frequency shifted toward lower values, whereas the TL decreased only slightly. These numerical findings are consistent with the experimental results obtained for the automotive-muffler assembly under mean-flow conditions, indicating that the observed low-frequency shift is primarily associated with the combined effects of duct geometry and resonator configuration.

4. Conclusions

In this study, we developed a reliable TL measurement method and verified its performance through theoretical analysis, numerical simulations, and experimental investigations. To improve measurement accuracy, a correction function based on the two-microphone transfer function

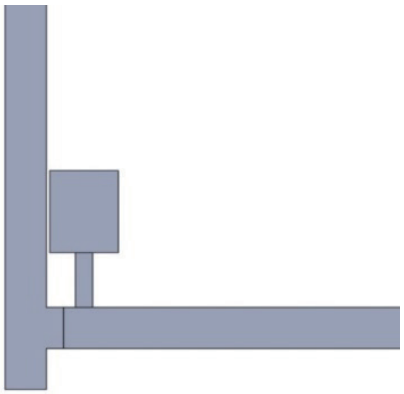


Fig. 36. (Color online) Schematic of the resonator setup near the pipe elbow.

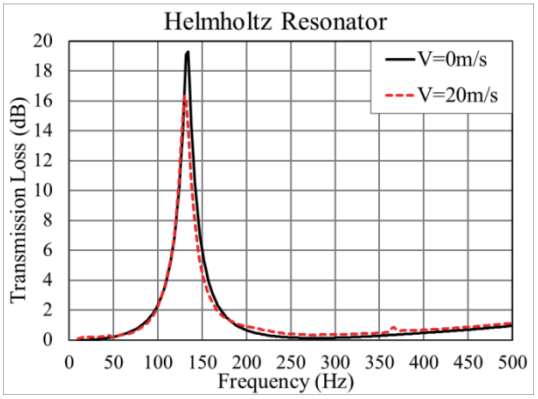


Fig. 37. (Color online) Analysis results of the Helmholtz resonator oriented in reverse and positioned adjacent to the pipe elbow.

method was incorporated into the proposed algorithm. The experimental results demonstrated that the corrected algorithm produced more accurate TL measurements than the conventional approach. On the basis of the four-pole parameter theory, a microphone-position-switching method was developed for TL measurements, whereas the two-load method was employed to verify the reliability of the experimental data. The proposed measurement procedure was shown to be valid and applicable to evaluating the acoustic performance of mufflers. The effects of mean flow on different muffler configurations were also investigated. The results indicated that mean flow increased the TL of a simple expansion chamber, and a similar improvement was observed for the inlet-extended expansion chamber. In contrast, the quarter-wavelength resonator exhibited reduced TL at its resonance frequency, whereas the Helmholtz resonator showed a decrease in TL accompanied by a shift in resonance frequency toward higher values. To improve the robustness of FRF correction, the arithmetic and geometric mean correction methods were compared. Although the arithmetic mean generated smoother TL curves under mean-flow conditions, the geometric mean achieved better agreement with both analytical predictions and numerical simulation results. Therefore, the geometric mean is recommended as a more appropriate correction function for TL measurements. Furthermore, the finite element simulations performed using COMSOL Multiphysics were in excellent agreement with the analytical and experimental results, demonstrating the effectiveness of the proposed numerical model. The combined use of numerical simulations and experimental validation provides an efficient approach to the design and optimization of mufflers. This methodology enables designers to evaluate acoustic performance during the early design stage, thereby reducing prototype development time and manufacturing costs while improving overall design efficiency.

References

1 M. L. Munjal and A. G. Doige: J. Sound Vib. **141** (1990) 323.
2 ASTM International: ASTM E1050-98, Standard Test Method for Impedance and Absorption of Acoustical Materials Using a Tube, Two Microphones, and a Digital Frequency Analysis System (ASTM International, West Conshohocken, PA, 2006).

3 S. H. Wu and M. H. Huang: Proc. 22nd Natl. Conf. Vib. Noise Eng. (2014) (in Chinese).
4 P. Chaitanya and M. L. Munjal: Appl. Acoust. **72** (2011) 65.
5 A. Selamet and I. J. Lee: J. Acoust. Soc. Am. **113** (2003) 1975.
6 E. S. Webster and C. E. Davies: Sensors **10** (2010) 10663.
7 H. Huang, Z. Chen, and Z. Ji: Adv. Mech. Eng. **11** (2019) 1.
8 H. Kim and A. Selamet: Int. J. Veh. Noise Vib. **7** (2011) 285.
9 E. Selamet, A. Selamet, A. Iqbal, and H. Kim: Int. J. Mater. Mech. Manuf. **1** (2013) 210.
10 H. Huang, Z. Ji, and K. Han: J. Theor. Comput. Acoust. **28** (2020) 1950015.
11 D. Guan, D. Zhao, and Z. Ren: Int. J. Aerosp. Eng. **2020** (2020) 8887463.
12 R. W. Fox, A. T. McDonald, P. J. Pritchard, and J. C. Leylegian: Fluid Mechanics (John Wiley & Sons, New York, 2012) 8th ed., pp. 42–43.
13 J. Y. Chung and D. A. Blaser: J. Acoust. Soc. Am. **68** (1980) 907.
14 C. S. Chang and C. H. Chang: Noise and Vibration Control (Gaoli Books, Taipei, 2016) 7th ed., p. 224 (in Chinese).
15 S. H. Crandall and W. D. Mark: Random Vibration in Mechanical Systems (Academic Press, New York, 1973) pp. 44–45.

About the Authors



Chang-Sheng Lin received his Ph.D. degree from the Department of Aeronautics and Astronautics of National Cheng Kung University, Taiwan, in 2011. He joined the Faculty of National Kaohsiung University of Science and Technology, Taiwan, in 2024, where he is currently an associate professor in the Department of Mechanical Engineering. His research interests are in random vibration and modal analysis. (changsheng@nkust.edu.tw)



Chin-Cheng Kang received his B.S. and M.S. degrees from the Department of Vehicle of National Pingtung University of Science and Technology, Taiwan, in 2019 and 2021, respectively. He is currently an engineer in the Outfitting Design Section, Department of Design, CSBC Corporation, Taiwan.